

pubs.acs.org/est Article

# Polymer Coatings Affect Transport and Remobilization of Colloidal Activated Carbon in Saturated Sand Columns: Implications for In Situ Groundwater Remediation

Xun Guan, Lingchen Kong, Chenwei Liu, Dimin Fan, Bridget Anger, William P. Johnson, Gregory V. Lowry, Guangbin Li, Anthony Danko, and Xitong Liu\*



Cite This: Environ. Sci. Technol. 2024, 58, 8531-8541



**ACCESS** I

III Metrics & More

Article Recommendations

s Supporting Information

ABSTRACT: Colloidal activated carbon (CAC) is an emerging technology for the in situ remediation of groundwater impacted by per- and polyfluoroalkyl substances (PFAS). In assessing the long-term effectiveness of a CAC barrier, it is crucial to evaluate the potential of emplaced CAC particles to be remobilized and migrate away from the sorptive barrier. We examine the effect of two polymer stabilizers, carboxymethyl cellulose (CMC) and polydiallyldimethylammonium chloride (PolyDM), on CAC deposition and remobilization in saturated sand columns. CMC-modified CAC showed high mobility in a wide ionic strength (IS) range from 0.1 to 100 mM, which is favorable for CAC delivery at a sufficient scale. Interestingly, the mobility of PolyDM-modified CAC was high at low IS (0.1 mM) but greatly reduced at high IS

Injection well			
Soil			
Water table		Transport distance	Remobilization after emplacement
PFAS plume Sorptive barrier	Bare CAC	short	low
	CMC - CAC	sufficient	significant
	PolyDM - CAC	ionic strength dependent	none

(100 mM). Notably, significant remobilization (release) of deposited CMC-CAC particles occurred upon the introduction of solution with low IS following deposition at high IS. In contrast, PolyDM-CAC did not undergo any remobilization following deposition due to its favorable interactions with the quartz sand. We further elucidated the CAC deposition and remobilization behaviors by analyzing colloid—collector interactions through the application of Derjaguin—Landau—Verwey—Overbeek theory, and the inclusion of a discrete representation of charge heterogeneity on the quartz sand surface. The classical colloid filtration theory was also employed to estimate the travel distance of CAC in saturated columns. Our results underscore the roles of polymer coatings and solution chemistry in CAC transport, providing valuable guidelines for the design of in situ CAC remediation with maximized delivery efficiency and barrier longevity.

KEYWORDS: colloidal activated carbon, transport, remobilization, polymer stabilizers, sand column

## **■** INTRODUCTION

As a cost-effective alternative to the traditional ex situ pump and treat technology for groundwater remediation, the application of in situ groundwater remediation through the injection of colloidal materials has gained considerable attention. Subsurface colloidal activated carbon (CAC) barriers are an emerging technology for the in situ remediation of groundwater sites impacted by per- and polyfluoroalkyl substances (PFAS).<sup>1-4</sup> AC exhibits exceptional adsorption capacity, making it suitable for constructing a highly efficient sorption barrier. The small size of CAC particles  $(0.5-2 \mu m)$ which is much smaller than other commercial AC (>10  $\mu$ m) allows for direct injection into permeable zones within aquifers, where the main PFAS mass flux occurs. The injected CAC particles are expected to distribute in the porous media, coat the aquifer matrix solids, and form a sorptive barrier to reduce PFAS flux and contain or halt plume migration downstream, 1-3 though the long-term performance of the in situ barriers remains to be further investigated.

Bare CAC particles without surface modification are colloidally unstable and tend to aggregate in water. Consequently, polymers are used as stabilizers to enhance the stability and mobility of CAC particles in subsurface environments, enabling in situ remediation via direct injection of CAC suspensions. Carboxymethyl cellulose (CMC) is a negatively charged polymer that has been widely applied as a stabilizer for particulate amendments (including CAC) in groundwater remediation.

Received: October 5, 2023 Revised: April 12, 2024 Accepted: April 16, 2024 Published: May 1, 2024





polymer polydiallyldimethylammonium chloride (PolyDM) was applied as a coating agent to improve the stability of powdered activated carbon particles during in situ remediation, 10 although the suitability of PolyDM as a stabilizer for CAC remains unknown. Presently, the primary uncertainties related to CAC-enabled in situ remediation are the transport distance during delivery and the potential for remobilization after CAC emplacement. The CAC must exhibit sufficiently high mobility to transport a sufficient distance from the injection point to establish an effective sorptive barrier. After the CAC particles are emplaced, it is crucial for the propensity of their long-term remobilization from the aquifer materials to be low, in order to maintain barrier longevity and prevent colloid-facilitated PFAS migration downgradient.

The remobilization of particles from a surface consists of two steps: (1) detachment of the particle from the surface and (2) transport of the detached particle into the bulk solution.<sup>11</sup> In coastal aquifers where many PFAS-impacted sites are located (reported in the PFAS interactive map created by the Environmental Working Group), 12 the constant exchange between freshwater and saline water driven by tidal pumping creates a fluctuation in groundwater ionic strength (IS). Therefore, the fluctuation results in the mixed coastal groundwater having an IS similar to that of brackish groundwater with a salinity of 1 to 10 g/L (17 to 170 mM as NaCl),14 which is lower than that of seawater (700 mM)<sup>15,16</sup> but higher than that of typical groundwater (2 to 5 mM). 17,18 In addition, during a rainfall or flooding event (typical IS in the rainwater ranged from 0.11 to 0.26 mM), <sup>19</sup> the groundwater IS can change substantially. When groundwater IS decreases, the increased electrostatic repulsion between the colloids and aquifer materials (e.g., sand) can cause the deposited CAC to be detached and released back into the aqueous phase. As polymer coatings can alter the surface charge of colloids and impart steric interactions, <sup>20</sup> it is expected that the coupling effects of polymer coating and IS will regulate the remobilization behaviors of CAC. However, while the deposition behaviors of particulate amendments (most notably zerovalent iron, ZVI)<sup>21–25</sup> in saturated porous media have been extensively studied, investigations on the remobilization of particulate amendments following their deposition are extremely limited. To date, we are unaware of studies that quantitatively assess the remobilization of CAC from sand surfaces. In addition, the mechanisms underlying the remobilization of CAC remain to be elucidated.

In this study, we fill the knowledge gap by investigating the deposition and remobilization behavior of bare and polymerstabilized CAC in packed saturated sand columns under different IS. We focus on answering two research questions: (1) How do different types of polymer coatings, including negatively charged CMC and positively charged PolyDM, affect the deposition of CAC in saturated porous media? (2) To what extent would the emplaced CAC with different polymer coatings get remobilized upon changing groundwater IS? Our results show that the coupling effects of the polymer coating and IS regulate the deposition and remobilization behaviors of CAC, which can be explained by colloid-surface interactions that include a discrete representation of surface charge heterogeneity. Our results highlight the crucial role of polymer stabilizers in controlling the transport of CAC amendments in saturated porous media and provide guidance for the selection of polymer coatings for designing in situ CAC

barriers with maximized amendment delivery efficiency and barrier longevity.

# ■ MATERIALS AND METHODS

Preparation of Polymer-Stabilized CAC. The CAC particles (Intraplex) were supplied in the form of a dry powder by Intrapore (Germany). Deionized (DI) water from a Milli-Q water system (18.2 M $\Omega$ ·cm, Millipore) was used to prepare all solutions. Sodium CMC (average molecular weight MW ~90,000 g/mol) and PolyDM (average MW 200,000-350,000 g/mol, 20 wt % in H<sub>2</sub>O) were purchased from Sigma-Aldrich and used without purification. To prepare bare CAC suspension, 50 mg of CAC powder was dispersed in 100 mL of DI water to obtain a CAC stock suspension of 500 mg/L. To prepare CAC stock suspensions with polymer coatings, 50 mg/L CMC or PolyDM was added into a 500 mg/L CAC suspension to achieve a polymer/CAC mass ratio of 1:10. All of the stock suspensions were subjected to sonication in an ultrasonic bath sonicator (Barnsonic, Emerson M1800) for 30 min to create stable suspensions.

**Porous Media.** Quartz sand is a primary component found in many coastal aquifer sites. <sup>26,27</sup> We used quartz sand (Sigma-Aldrich, 50–70 mesh) as the media for all column experiments. Based on the particle size and terminology adopted by the United States Department of Agriculture (USDA, 1993), this quartz sand falls within the range of fine sand and medium sand. <sup>28</sup> The commercial sand was first cleaned thoroughly to remove impurities and fine colloid matter using a protocol reported previously. <sup>29</sup> The detailed procedures for cleaning the sand are described in Text S1 in the Supporting Information.

Characterization of CAC and Quartz Sand. We used a Zetasizer (Malvern) to measure the hydrodynamic size and zeta potential of the CACs. The zeta potential was derived from the electrophoretic mobility using the Smoluchowski equation.<sup>30</sup> Details are shown in Text S2 in the Supporting Information. To further verify the particle diameters, the three CAC suspensions were dried on a silicon wafer and observed under scanning electron microscopy (SEM, see Text S3 in the Supporting Information for details). The size distributions of the CAC particles were analyzed using ImageJ.

**Sedimentation Kinetics of CAC.** Freshly prepared 500 mg/L CAC stock suspensions were diluted to 50 mg/L, subjected to ultrasonication for 20 min, and placed in a quartz cuvette (pH  $7.5 \pm 0.2$  buffered by 0.1 mM NaHCO<sub>3</sub>). The absorbance of bare CAC, CMC-CAC, and PolyDM-CAC was recorded over 6 h at wavelengths of 214, 218, and 220 nm, respectively, using a UV—vis spectrometer (Thermo Fisher Scientific, GENESYS 150). The sedimentation kinetics were presented as normalized concentration versus time. <sup>31</sup>

**CAC Column Transport Experiments.** We conducted column experiments to investigate (1) the transport of CAC in the saturated porous media and (2) the propensity for emplaced CAC particles to be remobilized upon a perturbation in solution chemistry. The CAC transport experiments were performed in glass chromatography columns (KIMBLE Flex-Column, inner diameter of 2.5 cm and length of 10 cm, Grainger) packed with cleaned quartz sand grains. The end of the column is equipped with a frit (porous disc), which serves to retain the packing media and ensure a uniform flow of the sample through the column with a minimal hold-up volume. The average diameter of the frit is around 30  $\mu$ m, significantly larger than the size of our CAC particles ( $d = 1 \mu$ m). Therefore, there is little risk of filtering out CAC particles.

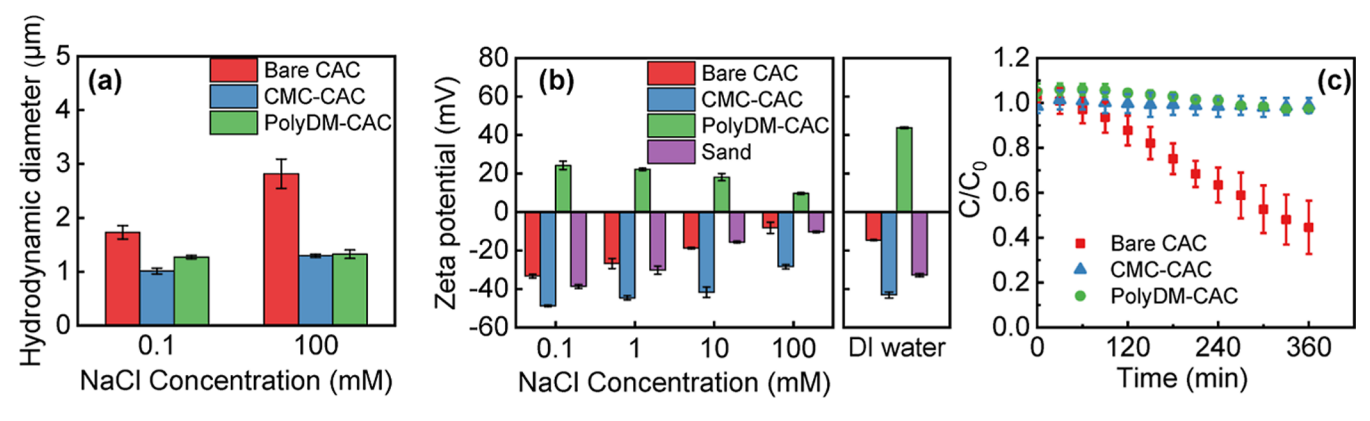


Figure 1. (a) Hydrodynamic diameter of bare CAC, CMC-CAC, and PolyDM-CAC under 0.1 and 100 mM NaCl at pH  $7.5 \pm 0.2$ . (b) Zeta potential of bare CAC, CMC-CAC, PolyDM-CAC, and quartz sand under 0.1, 1, 10, and 100 mM NaCl (adjusted pH at  $7.5 \pm 0.2$ ) and DI water (unadjusted pH  $5.8 \pm 0.2$ ). (c) Sedimentation kinetics of bare CAC, CMC-CAC, and PolyDM-CAC. Error bars indicate the standard deviation of duplicate measurements.

Clean and dry sand was packed into the column in five batches (20 g each batch) and then pressed tight to minimize air entrapment. After dry packing the columns, the pore volume (PV) of each column was determined by measuring the volume of air in the column excluding the sand (see Text S4 in Supporting Information). In all column experiments, freshly prepared 500 mg/L CAC stock suspension was diluted into 50 mg/L and sonicated for 20 min. While a much higher CAC injection concentration (typically  $\sim 10 \text{ g/L}$ ) is used in practical field applications, we used a concentration of 50 mg/L to avoid rapid particle aggregation and ripening effects associated with high CAC concentrations.<sup>22</sup> Under low CAC concentration, the conditions of clean bed filtration theory are satisfied, and the transport of CAC is controlled by colloid-collector interactions. Utilizing the clean bed filtration theory is important for assessing the risk of undesired migration away from the point of application, particularly in areas where low concentrations of CAC particles are anticipated at the periphery of the injection sites.<sup>32</sup> The time intervals between sonication and electrolyte addition as well as between electrolyte addition and injection of CAC suspensions into the column were kept consistent (15 min each) in all experiments.

Before the CAC transport experiments, the packed columns were first equilibrated with 10 PVs of DI water using a peristaltic pump (BT100-1L, Langer Instrument) with a flow velocity of 6.185 mL/min (corresponding to a superficial velocity of 0.021 cm/s, or 18 m/day) and then conditioned with 10 PVs of a buffered electrolyte solution (0.1 mM NaHCO<sub>3</sub>, pH adjusted at 7.5  $\pm$  0.2). We note that groundwater velocity of tens of meters per day is not uncommon in contaminated coastal sites.<sup>33</sup> The steady flow rate of the peristaltic pump is validated in Figure S1, excluding the potential influence of the pulses. Figure S2 in the Supporting Information shows the setup of the column study. A three-step procedure was used for the CAC deposition and remobilization experiment.<sup>29</sup> In step A (deposition step), 5 PVs CAC suspension (50 mg/L, pH 7.5  $\pm$  0.2) at different IS was fed continuously to the columns upward. In step B (rinse step), the columns were rinsed with 5 PVs of background electrolyte solution identical to that of the CAC suspension. Finally, in step C (remobilization step), the columns were rinsed with 5 PVs DI water (pH unadjusted at  $5.9 \pm 0.3$ ) to investigate the remobilization of the deposited

CAC upon a change in IS. The use of DI water in step C represents a worst-case scenario for colloid remobilization. The CAC concentration of effluent was monitored at 30 s intervals by measuring the absorbance using a UV-vis spectrophotometer (Thermo, Genesys150) with a 500  $\mu$ L quartz cuvette. The calibration curves for the CAC suspensions were obtained in both DI water and 100 mM NaCl to account for the effect of IS on CAC absorbance (Figure S3). In our control experiments, we found that rinsing a CAC-free sand column with DI water resulted in appreciable absorbance at 230 nm, which interfered with the measurement of CAC concentration. Therefore, we pretreated the sand column by rinsing the column with seven cycles of 100 mM NaCl and DI water after which the absorbance in the effluent was negligible (Figure S4) and then conducted the column transport experiments. We also conducted a tracer test using NaBr to aid the calculation of the deposition amount in step A and the remobilization amount in step C (see Text S5 in the Supporting Information for details).

**xDLVO Interaction Energy Profile.** To further understand the mechanisms for CAC deposition on and remobilization from the sand media, we calculated Extended Derjaguin-Landau-Verwey-Overbeek (xDLVO) interaction energy profiles using the Parti Suite-xDLVO package.34 The calculations involve the intrinsic assumption that both the CAC particles and quartz sand are spherical and of uniform size. The interaction between a CAC colloid and the sand grain surface (colloid-collector), as well as between two CAC colloids (colloid-colloid), was calculated as the sum of the van der Waals (vdW), electrical double layer (EDL), Born repulsion, Lewis acid-base (LAB), and steric interactions varying with separation distance.<sup>35</sup> In addition to using the mean-field representation, we explored how the presence of discrete heterogeneity (i.e., positively charged heterodomains) on the quartz sand affects colloid-collector interactions. Specific equations and parameters used for calculating these interactions are shown in Text S6.

#### RESULTS AND DISCUSSION

Characterization of Bare and Polymer-Stabilized CAC. We first measured the hydrodynamic size of bare, CMC-coated, and PolyDM-coated CAC particles at 0.1 and 100 mM NaCl using DLS. Figure 1a shows that the hydrodynamic diameter of bare CAC at 100 mM NaCl (2.8

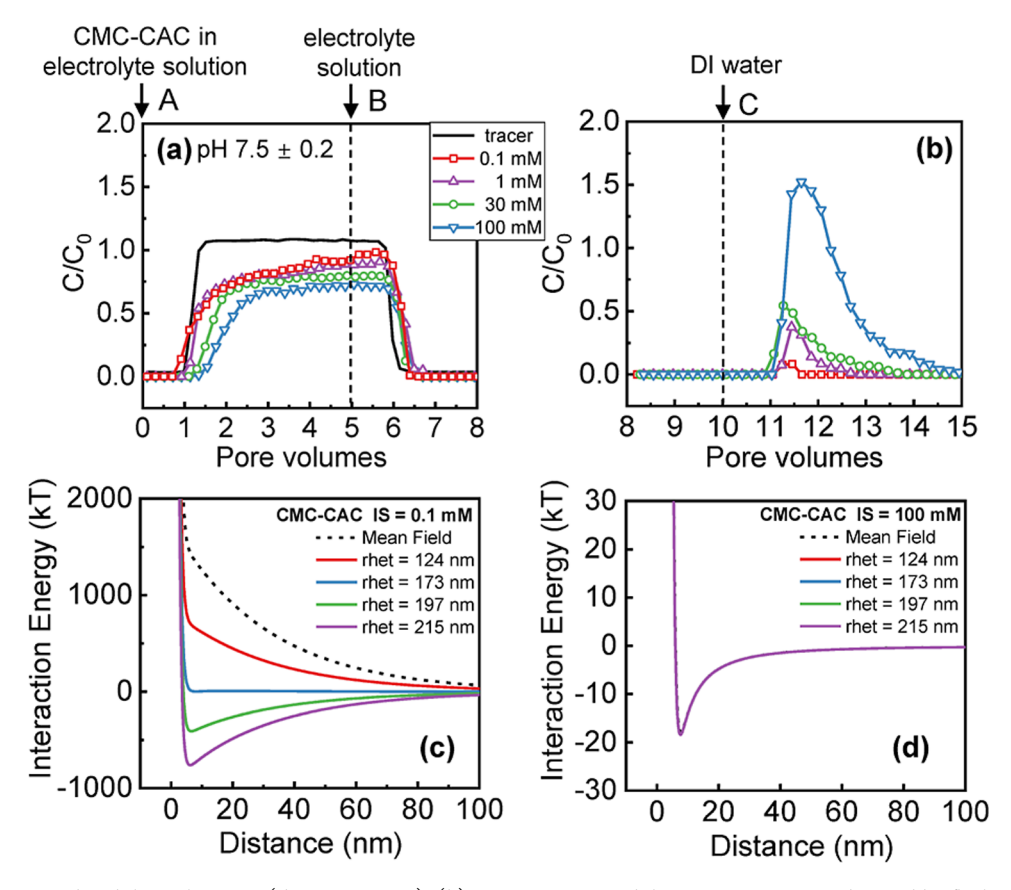


Figure 2. (a) CMC-CAC breakthrough curves (deposition step). (b) CMC-CAC remobilization curves were obtained by flushing columns with DI water following the deposition. Illustrations of the variation of interaction energy (colloid—collector interaction) over the mean field and various heterodomain radii (124, 173, 197, and 215 nm) between CMC-CAC and the sand surface at (c) 0.1 mM and (d) 100 mM IS as a function of separation distance. Dotted black lines are the interaction energy curves over the mean-field surfaces. "rhet" indicates heterodomain radii.

 $\pm$  0.3  $\mu$ m) was significantly higher (t-test, p = 0.017) than that at 0.1 mM NaCl (1.7  $\pm$  0.1  $\mu$ m). In comparison, for CMC-CAC and PolyDM-CAC, the measured hydrodynamic diameter was similar at 0.1 and 100 mM NaCl. These results indicate that bare CAC underwent significant aggregation, while the CAC particles with polymer coatings exhibited stronger stability when IS increased. We further verified the enhanced colloid stability of polymer-coated CAC particles using SEM imaging (Figure S5 in the Supporting Information). The SEM image of bare CAC shows large agglomerates of CAC particles, whereas the SEM images of polymer-modified CACs display predominantly well-dispersed particles. According to the size distribution analyzed based on SEM images, the bare CAC presents a larger particle size ranging from 0.5 to 10  $\mu$ m, while the polymer-modified CAC shows an average diameter of around 0.1 to 3  $\mu$ m, further confirming that both CMC and PolyDM polymers stabilized CAC particles in the suspensions.

We further characterized the surface charge of the CAC particles at pH 7.5  $\pm$  0.2 (Figure 1b). The bare CAC was negatively charged in the range of IS tested (0.1 mM to 100 mM NaCl), consistent with the isoelectric point of the CAC of 5.7 determined by Georgi et al.<sup>6</sup> The negative surface charge of the CAC particles originates from the dissociation of oxygencontaining acidic functional groups such as carboxyl groups. The CMC-CAC was more negatively charged than the bare CAC, due to more abundant carboxyl groups imparted by CMC. The PolyDM-CAC exhibited a positive charge over the IS range investigated, indicating that the PolyDM molecules

adsorbed on CAC and reversed the surface charge of the particle. All three CACs show a decreasing magnitude in zeta potential with the increase of IS because of charge screening at high IS.  $^{22,30}$  The zeta potential of the three CACs tested in DI water with an unadjusted pH of ca.  $5.9 \pm 0.3$  was slightly higher (less negative or more positive) than that measured at pH  $7.5 \pm 0.2$  with 0.1 mM NaCl. We attribute this to the higher degree of protonation of surface functional groups (carboxyl and amine) at lower pH.

In field application, a highly desirable characteristic for CAC suspensions is their stability against aggregation and sedimentation.<sup>5</sup> We examined the sedimentation kinetics of CAC with and without polymer coatings to gain further insights into their colloid stability. Over a period of 6 h, bare CAC settled down by more than 50%, while the CMC-CAC and PolyDM-CAC suspensions show almost no settling (Figure 1c). Additionally, to examine whether polymer desorption occurs during transport, we performed sedimentation kinetics testing on CMC-CAC collected from the effluent of the column transport experiment. Similar to the freshly prepared CMC-CAC suspension, we observed no significant sedimentation of CMC-CAC post-transport (Figure S6). This suggests that polymer-modified CAC retains high stability after transport; thus, the desorption of polymer during the transport process is likely negligible.

Our results demonstrated that bare CAC is prone to undergoing aggregation and sedimentation and, therefore, unsuitable for in situ remediation applications without polymer modification. The two polymer coatings significantly enhanced

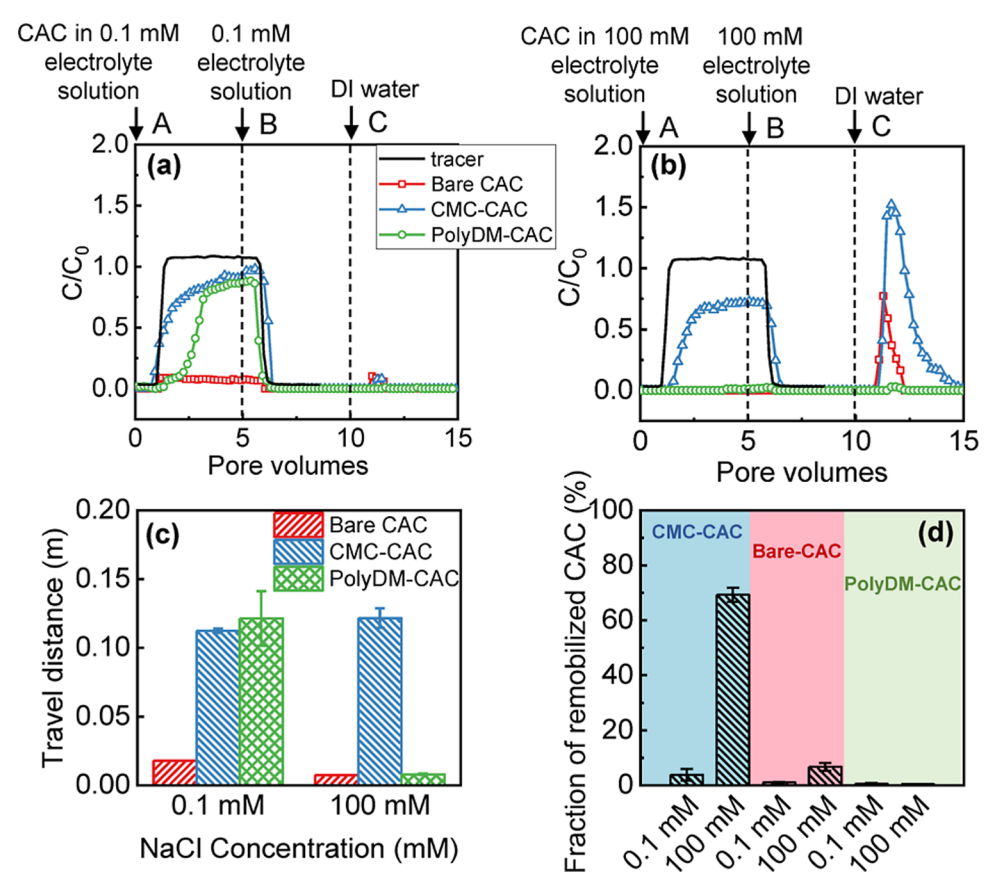


Figure 3. Bare CAC, CMC-CAC, and PolyDM-CAC breakthrough and remobilization curves when the deposition occurs at (a) 0.1 mM IS and (b) 100 mM IS, both at pH 7.5 ± 0.2. (c) Estimated travel distance of bare CAC, CMC-CAC, and PolyDM-CAC in the column at 0.1 and 100 mM IS. (d) Fraction of originally deposited CACs (%) that were remobilized from the column after flushing the column with DI water for 20 min.

the CAC particle stability, likely through two mechanisms: (1) electrostatic stabilization caused by the increased electrical double layer (EDL) repulsion and (2) the steric stabilization that occurs when the polymer segments interpenetrate each other and then increase the osmotic repulsive force, thereby enhancing the stability of colloid particles. The case of CMC-CAC, the CMC coating increases the negative charges on the CAC particle and thus enhances the EDL repulsion. Therefore, the combination of electrostatic and steric stabilization, or electrosteric stabilization, results in the enhanced colloid stability of CMC-CAC. The PolyDM-CAC, steric stabilization is likely the main mechanism for improving colloid stability.

Effect of IS on the Deposition of CMC-CAC: Mean Field Approach vs Surface Heterogeneity. In light of the wide application of CMC as a stabilizer for particulate amendments, 7-9 we first examined the transport behaviors of CMC-CAC at various IS (0.1 to 100 mM), to simulate the fluctuation of salinity in coastal areas. 13,41 Figure 2a presents CMC-CAC breakthrough curves plotted as the normalized effluent concentration against the number of PVs passed through the column. As IS increases, there is a discernible decline in the effluent concentration of CMC-CAC, signifying an increase in the deposition of particles on the sand. This phenomenon can be qualitatively understood by the charge screening effect under the DLVO theory: increasing IS reduces EDL repulsion but has negligible impact on dispersion contribution to the vdW attraction,<sup>42</sup> therefore reducing the energy barrier to deposition.<sup>30</sup>

We further simulated the xDLVO energy profiles of CMC-CAC interacting with quartz sand at 0.1 and 100 mM IS using a mean-field approach where the area-averaged surface potential is employed (dotted line shown in Figure 2c,d). However, while the deposition was observed in the column experiment for CMC-CAC at 0.1 mM IS (Figure 2a), the energy profile over the mean field (Figure 2c) shows a significant deposition energy barrier. Such a high deposition energy barrier cannot explain the observed attachment of CMC-CAC in the column. Previous studies on colloid transport have shown similar discrepancies between the DLVO theory and experimentally measured deposition rates. 43,44 To explain the discrepancy, different mechanisms have been invoked, including deposition in the secondary minimum, surface roughness, and surface charge heterogeneity. 43-45

Here, we evaluate whether the inclusion of discrete heterodomains (nanoscale zones of positive charge) allows prediction of the deposition of CMC-CAC colloids under unfavorable conditions. Given that xDLVO interactions exhibit their effects primarily within short distances (<200 nm), these interactions are confined to a finite zone of interaction (ZOI). For EDL interactions, ZOI is determined by solution IS and colloid radius (see Text S7). The finite interaction zone between colloids and surfaces represents a crucial factor in colloid—surface interactions. In the presence of surface charge heterogeneity, the ZOI can encompass a nanoscale region characterized by an attractive charge to the colloid (heterodomain). This can lead to a reduction in repulsion or

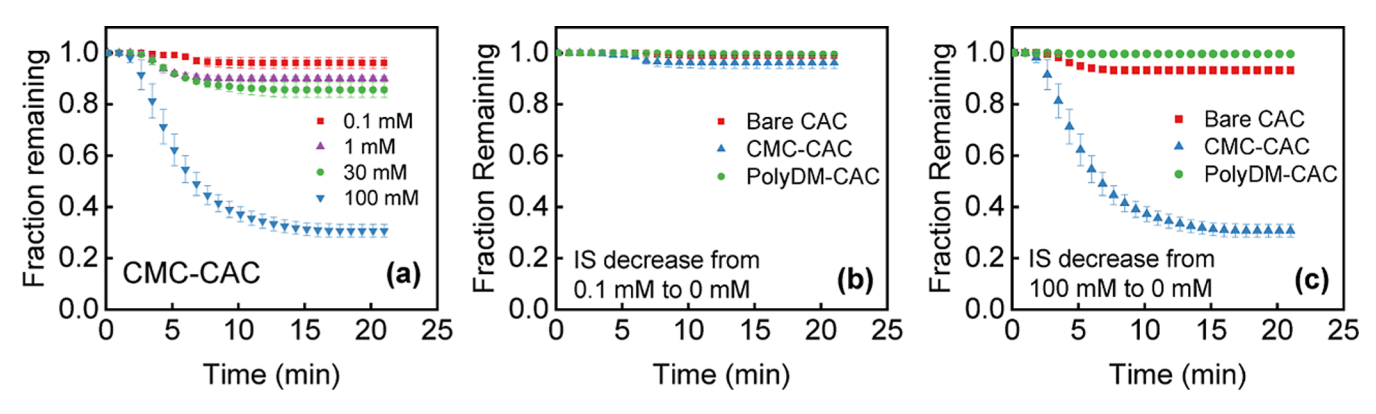


Figure 4. (a) Fraction of originally deposited CMC-CAC (%) in the column that remained in the column upon the introduction of DI water as a function of time. The different NaCl concentrations indicate the IS during the deposition step. Fraction of the originally deposited bare, CMC-CAC, and PolyDM-CAC (%) that remained in the column upon the introduction of DI water following deposition at (b) 0.1 and (c) 100 mM.

even a reversal of repulsion into attraction, contingent upon the extent of overlap between the heterodomain and the ZOI.

We plotted the xDLVO energy profiles in the presence of representative heterodomains with varied sizes (124, 173, 197, and 215 nm). As the heterodomain radius increased, we observed a remarkable reduction in the deposition energy barrier (Figure 2c). Notably, when the heterodomain radius exceeded 173 nm, the deposition energy barrier completely vanished. These simulations support the role of heterogeneity in governing the attachment of CMC-CAC under unfavorable conditions at low IS. For a high IS of 100 mM, however, the energy profiles for the mean field and with different radii of heterodomain overlap (Figure 2d). This is because the examined heterodomain radius is larger than the ZOI, resulting in a fraction of heterodomain over ZOI equal to 1.35 As such, the inclusion of surface heterogeneity on the sand surface leads to the successful prediction of the deposition of CMC-CAC at both low and high IS.

Effects of Polymer Coatings on CAC Deposition and Transport Distance. The breakthrough curves depicted in Figure 3a,b illustrate the normalized concentration profiles of bare CAC, CMC-CAC, and PolyDM-CAC plotted as a function of the pore volumes passed through the column. Under deposition conditions of 0.1 mM NaCl at pH 7.5, both CMC-CAC and PolyDM-CAC exhibit lower levels of deposition compared with bare CAC. Based on the size characterization (Figure 1a), bare CAC is inherently unstable and prone to form larger aggregates. The observed higher fraction of deposition for aggregated bare CAC is consistent with clean bed filtration theory where the removal efficiency of the filter increases as the particle size surpasses approximately 1 μm due to the increase in transport efficiency by sedimentation.

The equilibrium breakthrough concentrations of CMC-CAC and PolyDM-CAC at 0.1 mM IS did not exhibit a significant difference (Figure 3a). Interestingly, the breakthrough of PolyDM-CAC was significantly delayed compared with that of the NaBr tracer test, and the effluent concentration gradually increased. We attribute this to the opposite charge of PolyDM-CAC to the quartz sand as well as the blocking mechanism. Due to the attractive interactions with the quartz sand, PolyDM-CAC undergoes favorable, mass-transport-limited deposition. As more PolyDM-CAC colloids deposit on the collector surface, the repulsive EDL interaction emanating from the deposited colloids (colloid—colloid interactions) can impede the subsequent deposition of additional colloids. As a

result, the effluent concentration gradually increases over time. 48–50 We further calculated the xDLVO energy profile of the colloid—colloid interaction for PolyDM-CAC. At 0.1 mM IS (Figure S7), the interaction energy indeed shows a large energy barrier to prevent colloid deposition, thus supporting the hypothesis of a blocking mechanism.

For the deposition at 100 mM IS (Figure 3b), bare CAC and PolyDM-CAC both show almost 100% deposition at 100 mM NaCl. The significant deposition observed under such conditions may hinder the emplacement of CAC for in situ remediation, as the CAC particles will accumulate and deposit on the aquifer matrix at the injection site. Consequently, they will fail to transport sufficient distances to form effective sorptive barriers. In contrast, approximately, 30% of the CMC-CAC particles were able to traverse through the column. The high deposition of bare CAC at high IS can be understood by its high tendency for aggregation, as discussed earlier. For PolyDM-CAC, based on the xDLVO interaction energy profile in Figure S7, the repulsive colloid-colloid interaction energy barrier vanishes at 100 mM due to charge screening; therefore, the above-mentioned blocking mechanism becomes insignificant at high IS. Therefore, PolyDM-CAC undergoes high deposition on the quartz sand due to attractive colloidcollector interactions.

We further employed colloid filtration theory to estimate and compare their respective travel distances under low and high IS. The relative transport distance (Z) is quantified according to eq 1 which is converted from the classical colloid filtration theory (details are shown in Text S8)

$$Z = -\ln\left(\frac{C_{\text{out}}}{C_{\text{in}}}\right) \frac{2d_{\text{c}}}{3(1-\varepsilon)\alpha\eta}$$
 (1)

where  $C_{\rm out}$  is the effluent breakthrough concentration,  $C_{\rm in}$  is the initial concentration,  $\alpha$  is the attachment efficiency,  $d_{\rm c}$  is the collector diameter, and  $\varepsilon$  is the porosity of the column.  $^{22,47}$  $\eta$  is the single collector efficiency, combining interception, diffusion, and sedimentation mechanisms. By utilizing the determined  $(C_{\rm out}/C_{\rm in})$  ratios from the column studies, along with the column properties  $(d_{\rm c},\varepsilon)$ , we estimated the  $\alpha\eta$  values for the three CACs at 0.1 and 100 mM NaCl. Subsequently, we calculated the travel distances necessary to remove 99% of the particles  $(C_{\rm out}/C_{\rm out}=0.01)$ , as depicted in Figure 3c. Among the three CACs, CMC-CAC shows the greatest travel distance at low and high IS. In comparison, bare CAC exhibits poor mobility regardless of the IS. The travel distance of PolyDM-

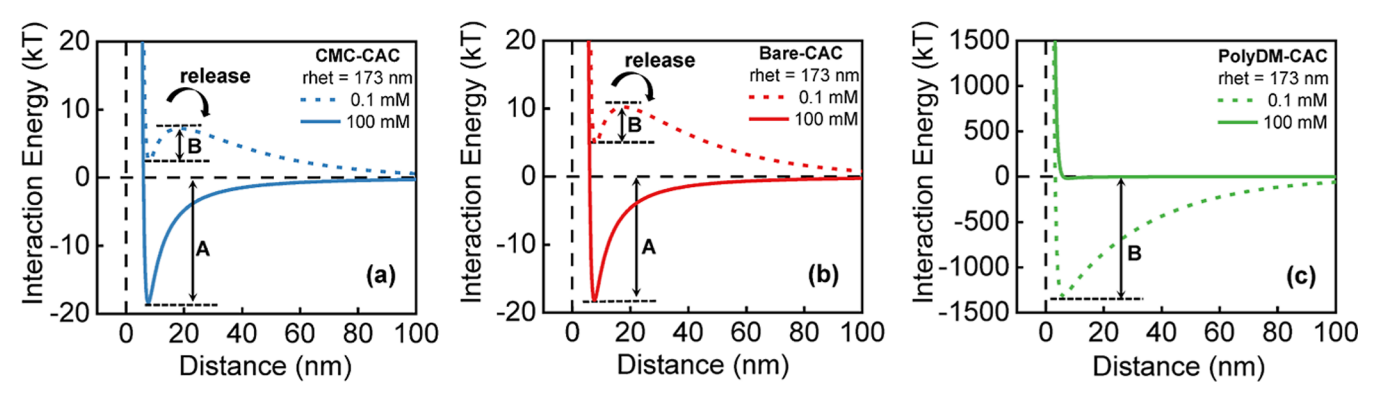


Figure 5. Illustrations of the variation of interaction energy (colloid–collector interaction) between (a) CMC-CAC, (b) unaggregated bare CAC (particle diameter =  $1.2 \mu m$ ), and (c) PolyDM-CAC and sand surface over 173 nm heterodomain radii at 0.1 and 100 mM IS as a function of separation distance (nm). The zeta potential and particle size measured in Figure 1 were used in the calculations. Detailed calculations are shown in Text S6 in the Supporting Information. For calculating the xDLVO energy profile of bare CAC, we employed the size of unaggregated bare CAC. This choice was made based on a study which reports that the size of the primary particle is a better proxy to evaluate colloidal interaction than the gyration radius of the aggregate.  $^{53}$ 

CAC is comparable to that of CMC-CAC at 0.1 mM IS, but significantly reduced at a higher IS of 100 mM. We note that due to the limitations imposed by the size of the columns, the estimated travel distance we obtained might not accurately reflect the actual travel distance of CAC in field remediation sites. The calculated travel distance is used solely for comparing different polymer coatings. The actual travel distance of CAC at field sites depends on several factors, including CAC concentration, groundwater solution chemistry, and flow, as well as the properties of the aquifer materials.

Impacts of Polymer Coatings on CAC Remobilization upon Reduction of Solution IS. Following the deposition (A) and rinse (B) steps, the column underwent a DI water rinse to induce the remobilization of CAC (step C, Figures 2b, and 3b). In the remobilization step (step C), we used DI water (pH unadjusted at  $5.9 \pm 0.3$ ) to simulate the scenario when the IS of groundwater substantially decreases following a rainfall or flooding event. We calculated the amount of deposited colloid during step A and the amount of remobilized colloid during step C. Subsequently, we plotted the remaining fraction of three CACs in the column as a function of time, as shown in Figure 4.

During rinsing of the column with DI water, a noticeable remobilization of CMC-CAC was observed. After about 10 to 15 min, the remobilization process reached a plateau (Figure 4a). The extent of remobilization for CMC-CAC increased with the magnitude of the change in the IS (Figure S8). Comparing CACs with different coatings, the three CACs all show insignificant remobilization when the solution was switched from 0.1 mM NaCl to DI water (Figure 4b), due to the small change in IS. When the IS decreased from 100 mM to about 0 mM (DI water), the fraction of remobilized CMC-CAC and bare CAC both increased, with CMC-CAC having the highest extent of remobilization (Figure 3d and 4c). In comparison, no observable remobilization occurred for PolyDM-CAC in both cases. This result suggests that the use of PolyDM as a polymer coating can effectively prevent the potential remobilization of the CAC particles from the sorptive barrier at coastal sites with constantly fluctuating groundwater

**Remobilization Mechanisms.** To obtain deeper insights into the mechanisms underlying the observed remobilization of CACs, we plotted the colloid—collector interaction energy

profiles in the presence of heterodomains (Figure 5). The radius of the heterodomain was chosen as 173 nm, which allows a successful explanation of the deposition behaviors of the CMC-CAC colloids (Figure 2c). In the presence of Born repulsion, LAB interaction, and steric forces, the difference in the energy level between the energy maximum and primary minimum, which is finite and surmountable, is the energy barrier for the remobilization of deposited colloids (Figure 5).

There are three possible mechanisms for understanding the remobilization of negatively charged bare and CMC-coated CAC. (1) As the IS decreases, the repulsion between likecharged surfaces increases, resulting in a reduction of the remobilization energy barrier from A to B (Figure 5a,b) and thus a higher tendency for the remobilization of CAC particles. (2) Based on torque balance theory, the deposited colloids will be remobilized when the driving torque caused by fluid drag can overcome the resisting torque (caused by colloid-collector attraction). 51,52 The reduction in IS leads to a smaller resisting torque and, therefore, induces colloid remobilization. Simultaneously, reducing the flow velocity decreases fluid drag, thereby diminishing particle mobility and resulting in increased deposition, while also reducing colloid remobilization, as shown in Figure S9. (3) The presence of heterodomain also substantially influences the colloidal remobilization process. The decrease in IS leads to an expansion of ZOI for EDL interactions (see Text S7). Subsequently, the reduction in the fraction of heterodomain over ZOI enhances the repulsive energy barrier, thus contributing to the enhanced remobilization under reduced IS conditions.<sup>35</sup>

For PolyDM-CAC, the adhesion between PolyDM-CAC and sand surfaces causes a deep primary minimum as well as a high remobilization energy barrier at low IS. Decreasing the IS results in an even higher remobilization energy barrier (Figure 5c), which prevents the remobilization of PolyDM-CAC from the sand surfaces. This supports the observation of no remobilization for PolyDM-CAC upon reduction of the IS.

The xDLVO analysis shows that the observed results are qualitatively in agreement with colloid attachment to and remobilization from the primary minimum when Born repulsion, LAB interaction, and steric forces are accounted for with the inclusion of discrete heterogeneity on the quartz sand surface. The surface charge heterogeneity of quartz sand can be attributed to the nonuniform ionization of surface

hydroxyl groups<sup>54</sup> and the possible presence of metal oxides.<sup>55</sup> To verify this, we conducted energy-dispersive X-ray spectroscopy testing using scanning electron microscopy (SEM-EDS) on the cleaned quartz sand used in the column experiment. We conducted multiple EDS point analyses on the surface of the sand. The results consistently show the presence of approximately 5% Al on the sand surface as well as traces of Mg and K (Figure S10). These results suggest the likely presence of metal oxides, such as Al<sub>2</sub>O<sub>3</sub> and MgO, on the sand surface. The presence of these positively charged metal oxides renders the sand surface heterogeneous in charge, aligning with our assumptions regarding colloidal interaction modeling. An alternative mechanism is colloid attachment and remobilization occurring within the secondary minimum, in which case colloids are retained in the column but are distant from the sand surfaces (a few nm to tens of nm).<sup>56</sup> In our xDLVO simulations, we did not observe the presence of a secondary minimum in the interaction energy profiles between quartz sand and CACs, suggesting that this mechanism is likely to be insignificant. The use of direct observation techniques (such as impinging jet) to visualize colloid translation on flat surfaces can help further elucidate the roles of primary and secondary minima in colloid retention and remobilization. 52,57

Transport of CMC-CAC in Actual Coastal Groundwater. We further conducted column experiments using groundwater collected from a PFAS-impacted coastal site (Figure S11). The conductivity of the groundwater sample was measured as 7830  $\mu$ S/cm. Then, we convert the conductivity (EC) to the IS according to the linear regression model reported by Griffin and Jurinak, 58,59 the details are shown in Table S1. Accordingly, the IS of the coastal groundwater sample was estimated as approximately 102 mM. Approximately, 70% of the CMC-CAC is deposited on the sand after injection into the columns in the coastal groundwater. During the DI water rinse, a remobilization of approximately 15% was observed, which was attributed to the decrease in IS. In addition, we conducted column experiments with varying pH levels during the remobilization step, using DI water at its unadjusted pH (5.9  $\pm$  0.3) and DI water with pH adjusted by NaHCO<sub>3</sub> to match that of coastal groundwater (7.5  $\pm$  0.2). As shown in Figure S11, the slight variations in pH did not significantly affect the remobilization of CAC. Overall, the results show that CAC exhibits significant deposition under high IS conditions (coastal groundwater), with some degree of remobilization occurring as the IS decreases. This is consistent with the trends observed in the NaCl solutions (Figure 2). Due to the complex chemical composition of coastal groundwater, the extent of deposition and remobilization differs from that in NaCl solutions, which warrants further study.

Implications for In Situ Remediation of Groundwater. For CAC-enabled in situ remediation of PFAS-impacted groundwater, the ideal scenario is to ensure sufficient mobility of CAC colloid in the subsurface environment to create large and effective sorptive barriers and to minimize remobilization of CAC particles after emplacement to reduce the secondary impacts caused by the potential downgradient migration of CAC particles. Under low IS of 0.1 mM, CMC-CAC and PolyDM-CAC can travel through the column which presents high mobility, while the majority of the bare CAC are deposited quickly after injection due to its high tendency for aggregation. Aggregated CAC could lead to obstruction in the injection nozzle and/or the surrounding soil matrix, consequently altering the hydraulic and geological conditions in

the area. At high IS of 100 mM representative of coastal brackish water, 100% deposition of bare CAC and PolyDM-CAC in the sand column was observed, which suggests low mobility of the CAC colloid and short travel distance after injection. In comparison, CMC-CAC has relatively higher mobility at both low and high IS, which makes CMC a more favorable polymer coating when high mobility of the CAC is desired in a wide range of groundwater salinity.

Coastal aquifers typically exhibit tidal pumping, i.e., the shifting of the fresh/saline interface, which causes a fluctuating IS. A considerable fraction of deposited CMC-CAC was remobilized as the IS decreased, suggesting that the potential downstream migration of CAC particles needs to be considered in practical barrier design. For positively charged PolyDM-CAC, no remobilization was observed when the solution IS reduced due to its strong attraction with the quartz sand surface. Overall, the two polymer-modified CACs both improve the stability of CAC suspensions and transport in saturated porous media, with the CMC performing the best at improving particle mobility and ensuring sufficient delivery distance. In cases where sites exhibit significant fluctuations in IS conditions and require minimal remobilization of CAC to ensure barrier longevity, positively charged polymers like PolyDM would be the preferred CAC stabilizers. We acknowledge that other constituents in groundwater, including divalent cations and natural organic matter, are also likely to play key roles in regulating CAC transport, which will be the focus of our future research. In addition, actual aquifer materials likely contain other minerals (such as iron oxide and calcium carbonate) and less uniform particles; 25,60-63 as such, the impacts of the heterogeneity of porous media on CAC delivery and remobilization need to be considered in the future

#### ASSOCIATED CONTENT

## Supporting Information

The Supporting Information is available free of charge at https://pubs.acs.org/doi/10.1021/acs.est.3c08251.

Quartz sand cleaning protocol, zeta potential measurements, SEM measurement, PV calculation, NaBr tracer test, equations for calculating xDLVO interactions, ZOI calculation, classical colloid filtration theory, geochemical characteristics of PFAS-impacted coastal groundwater, instantaneous flow velocity check of the peristaltic pump, column transport setup, calibration curves of three CACs, sand column pretreatment, SEM images and size distribution analysis, sedimentation kinetics of CMC-CAC within 6 h before and after transport, illustrations of the variation of the interaction energy between PolyDM-CAC colloids, fraction of CMC-CAC remobilized from the column, CMC-CAC column experiment using low flow velocity (1 mL/min), sand surface SEM-EDS point analysis, and CMC-CAC column experiment using coastal groundwater (PDF)

#### AUTHOR INFORMATION

## **Corresponding Author**

Xitong Liu — Department of Civil & Environmental Engineering, George Washington University, Washington, Washington D.C. 20052, United States; orcid.org/0000-0002-5197-3422; Email: xitongliu@gwu.edu

#### Authors

- Xun Guan Department of Civil & Environmental Engineering, George Washington University, Washington, Washington D.C. 20052, United States
- Lingchen Kong Department of Civil & Environmental Engineering, George Washington University, Washington, Washington D.C. 20052, United States
- Chenwei Liu Department of Civil & Environmental Engineering, George Washington University, Washington, Washington D.C. 20052, United States
- Dimin Fan Geosyntec Consultants, Inc, Columbia, Maryland 21044, United States
- Bridget Anger Department of Civil & Environmental Engineering, George Washington University, Washington, Washington D.C. 20052, United States
- William P. Johnson Department of Geology and Geophysics, University of Utah, Salt Lake City, Utah 84112, United States; © orcid.org/0000-0003-3126-3877
- Gregory V. Lowry Department of Civil & Environmental Engineering, Carnegie Mellon University, Pittsburgh, Pennsylvania 15213, United States; orcid.org/0000-0001-8599-008X
- Guangbin Li Department of Civil and Environmental Engineering, University of Maryland, College Park, Maryland 20742, United States
- Anthony Danko Naval Facilities Engineering Systems Command - Engineering and Expeditionary Warfare Center, Port Hueneme, California 93043, United States

Complete contact information is available at: https://pubs.acs.org/10.1021/acs.est.3c08251

#### **Notes**

The authors declare no competing financial interest.

### ACKNOWLEDGMENTS

The authors thank Dr. Julian Bosch (Intrapore) for supplying the colloidal activated carbon and Dr. Erik Rodriguez at GW for the use of Zetasizer. We also thank Dr. Katrin Mackenzie (Helmholtz Centre for Environmental Research), Dr. Julian Bosch (Intrapore), Dr. Mike Kavanaugh (Geosyntec), Dr. James Wang (Geosyntec), Rachel Molé (CMU), and Liu Jiang (UMD) for providing feedback on research plans and activities. This work was supported by the Strategic Environmental Research and Development Program (SERDP, Grant no. ER21-1070). We also gratefully acknowledge financial support from the American Chemical Society Petroleum Research Fund Doctoral New Investigator Grant (ACS-PRF Award #61735-DNI5 to X.L.).

#### REFERENCES

- (1) McGregor, R. In situ treatment of PFAS-impacted groundwater using colloidal activated carbon. *Remediation* **2018**, 28 (3), 33-41.
- (2) Carey, G. R.; McGregor, R.; Pham, A. L. T.; Sleep, B.; Hakimabadi, S. G. Evaluating the longevity of a PFAS in situ colloidal activated carbon remedy. *Remediation* **2019**, 29 (2), 17–31.
- (3) Carey, G. R.; Hakimabadi, S. G.; Singh, M.; McGregor, R.; Woodfield, C.; Van Geel, P. J.; Pham, A. L. T. Longevity of colloidal activated carbon for in situ PFAS remediation at AFFF-contaminated airport sites. *Remediation* **2022**, *33* (1), 3–23.
- (4) Hakimabadi, S. G.; Taylor, A.; Pham, A. L.-T. Factors affecting the adsorption of per-and polyfluoroalkyl substances (PFAS) by colloidal activated carbon. *Water Res.* **2023**, 242, 120212.

- (5) Fan, D.; Gilbert, E. J.; Fox, T. Current state of in situ subsurface remediation by activated carbon-based amendments. *J. Environ. Manage.* **2017**, 204, 793–803.
- (6) Georgi, A.; Schierz, A.; Mackenzie, K.; Kopinke, F.-D. Colloidal activated carbon for in-situ groundwater remediation Transport characteristics and adsorption of organic compounds in water-saturated sediment columns. *J. Contam. Hydrol.* **2015**, *179*, 76–88.
- (7) Kocur, C. M.; Lomheim, L.; Boparai, H. K.; Chowdhury, A. I.; Weber, K. P.; Austrins, L. M.; Edwards, E. A.; Sleep, B. E.; O'Carroll, D. M. Contributions of abiotic and biotic dechlorination following carboxymethyl cellulose stabilized nanoscale zero valent iron injection. *Environ. Sci. Technol.* 2015, 49 (14), 8648–8656.
- (8) Kocur, C. M.; Lomheim, L.; Molenda, O.; Weber, K. P.; Austrins, L. M.; Sleep, B. E.; Boparai, H. K.; Edwards, E. A.; O'Carroll, D. M. Long-term field study of microbial community and dechlorinating activity following carboxymethyl cellulose-stabilized nanoscale zero-valent iron injection. *Environ. Sci. Technol.* **2016**, *50* (14), 7658–7670.
- (9) Asad, M. A.; Khan, U. T.; Krol, M. M. Subsurface transport of carboxymethyl cellulose (CMC)-stabilized nanoscale zero valent iron (nZVI): Numerical and statistical analysis. *J. Contam. Hydrol.* **2021**, 243, 103870.
- (10) Liu, C.; Hatton, J.; Arnold, W. A.; Simcik, M. F.; Pennell, K. D. In Situ Sequestration of Perfluoroalkyl Substances Using Polymer-Stabilized Powdered Activated Carbon. *Environ. Sci. Technol.* **2020**, *54* (11), 6929–6936.
- (11) Ryan, J. N.; Gschwend, P. M. Effects of Ionic-Strength and Flow-Rate on Colloid Release Relating Kinetics to Intersurface Potential-Energy. *J. Colloid Interface Sci.* **1994**, *164* (1), 21–34.
- (12) PFAS Interactive Map. EWG Organization, https://www.ewg.org/interactive-maps/pfas\_contamination/map/(accessed Feb, 2024).
- (13) Liu, Y.; Jiao, J. J.; Liang, W.; Luo, X. Tidal pumping-induced nutrients dynamics and biogeochemical implications in an intertidal aquifer. *J. Geophys. Res.: Biogeosci.* **2017**, *122* (12), 3322–3342.
- (14) Brackish Groundwater Assessment; July; USGS, https://www.usgs.gov/mission-areas/water-resources/science/brackish-groundwater-assessment (accessed July 22, 2021).
- (15) Dos Santos, M. M. C.; Gonçalves, M. Electroanalytical chemistry of copper, lead and zinc complexes of amino acids at the ionic strength of seawater (0.70 M NaClO4 part III). *J. Electroanal. Chem. Interfacial Electrochem.* 1986, 208 (1), 137–152.
- (16) Liu, X.; Millero, F. J. The solubility of iron in seawater. *Mar. Chem.* **2002**, 77 (1), 43–54.
- (17) Tosco, T.; Bosch, J.; Meckenstock, R. U.; Sethi, R. Transport of Ferrihydrite Nanoparticles in Saturated Porous Media: Role of Ionic Strength and Flow Rate. *Environ. Sci. Technol.* **2012**, *46* (7), 4008–4015.
- (18) Li, Q.; Logan, B. E. Enhancing bacterial transport for bioaugmentation of aquifers using low ionic strength solutions and surfactants. *Water Res.* **1999**, 33 (4), 1090–1100.
- (19) Kumar, R.; Kumar, R.; Singh, A.; Arif, M.; Kumar, P.; Kumari, A. Chemometric approach to evaluate the chemical behavior of rainwater at high altitude in Shaune Garang catchment, Western Himalaya. *Sci. Rep.* **2022**, *12* (1), 12774.
- (20) Benjamin, M. M.; Lawler, D. F. Water Quality Engineering: Physical/chemical Treatment Processes; John Wiley & Sons, 2013.
- (21) Johnson, R. L.; Nurmi, J. T.; O'Brien Johnson, G. S.; Fan, D.; O'Brien Johnson, R. L.; Shi, Z.; Salter-Blanc, A. J.; Tratnyek, P. G.; Lowry, G. Field-scale transport and transformation of carboxymethylcellulose-stabilized nano zero-valent iron. *Environ. Sci. Technol.* **2013**, *47* (3), 1573–1580.
- (22) Saleh, N.; Kim, H.-J.; Phenrat, T.; Matyjaszewski, K.; Tilton, R. D.; Lowry, G. Ionic strength and composition affect the mobility of surface-modified Fe<sup>0</sup> nanoparticles in water-saturated sand columns. *Environ. Sci. Technol.* **2008**, 42 (9), 3349–3355.
- (23) Krol, M. M.; Oleniuk, A. J.; Kocur, C. M.; Sleep, B. E.; Bennett, P.; Xiong, Z.; O'Carroll, D. M. A field-validated model for in situ

- transport of polymer-stabilized nZVI and implications for subsurface injection. *Environ. Sci. Technol.* **2013**, 47 (13), 7332–7340.
- (24) Lefevre, E.; Bossa, N.; Wiesner, M. R.; Gunsch, C. K. A review of the environmental implications of in situ remediation by nanoscale zero valent iron (nZVI): behavior, transport and impacts on microbial communities. *Sci. Total Environ.* **2016**, *565*, 889–901.
- (25) Phenrat, T.; Cihan, A.; Kim, H.-J.; Mital, M.; Illangasekare, T.; Lowry, G. V. Transport and deposition of polymer-modified Fe<sup>0</sup> nanoparticles in 2-D heterogeneous porous media: effects of particle concentration, Fe<sup>0</sup> content, and coatings. *Environ. Sci. Technol.* **2010**, 44 (23), 9086–9093.
- (26) Aguila, J. F.; McDonnell, M. C.; Flynn, R.; Hamill, G. A.; Ruffell, A.; Benner, E. M.; Etsias, G.; Donohue, S. Characterizing groundwater salinity patterns in a coastal sand aquifer at Magilligan, Northern Ireland, using geophysical and geotechnical methods. *Environ. Earth Sci.* 2022, 81 (8), 231.
- (27) Trapp, H.; Horn, M. A. Ground Water Atlas of the United States: Segment 11, Delaware, Maryland, New Jersey, North Carolina, Pennsylvania, Virginia, West Virginia, 1997.
- (28) Blott, S. J.; Pye, K. Particle size scales and classification of sediment types based on particle size distributions: Review and recommended procedures. *Sedimentology* **2012**, *59* (7), 2071–2096.
- (29) Jaisi, D. P.; Saleh, N. B.; Blake, R. E.; Elimelech, M. Transport of Single-Walled Carbon Nanotubes in Porous Media: Filtration Mechanisms and Reversibility. *Environ. Sci. Technol.* **2008**, 42 (22), 8317–8323.
- (30) Elimelech, M.; Gregory, J.; Jia, X. Particle Deposition and Aggregation: Measurement, Modelling and Simulation; Butterworth-Heinemann, 2013.
- (31) Feng, Y.; Liu, X.; Huynh, K. A.; McCaffery, J. M.; Mao, L.; Gao, S.; Chen, K. L. Heteroaggregation of graphene oxide with nanometerand micrometer-sized hematite colloids: Influence on nanohybrid aggregation and microparticle sedimentation. *Environ. Sci. Technol.* 2017, 51 (12), 6821–6828.
- (32) Phenrat, T.; Kim, H.-J.; Fagerlund, F.; Illangasekare, T.; Tilton, R. D.; Lowry, G. V. Particle size distribution, concentration, and magnetic attraction affect transport of polymer-modified Fe<sup>0</sup> nanoparticles in sand columns. *Environ. Sci. Technol.* **2009**, 43 (13), 5079–5085.
- (33) Guaraglia, D. O.; Mayosky, M. A.; Pousa, J. L.; Kruse, E. E. Numerical and experimental study of a thermal probe for measuring groundwater velocity. *Rev. Sci. Instrum.* **2008**, *79* (1), 015102.
- (34) Parti-Suite Software. https://wpjohnsongroup.utah.edu/trajectoryCodes.html (accessed 2023 June).
- (35) Johnson, W. P.; Pazmiño, E. F. Colloid (Nano-and Microparticle) Transport and Surface Interaction in Groundwater; Groundwater Project, 2023. https://gw-project.org/books/colloid-nano-and-micro-particle-transport-and-surface-interaction-in-groundwater/.
- (36) Lin, S.; Cheng, Y.; Liu, J.; Wiesner, M. R. Polymeric Coatings on Silver Nanoparticles Hinder Autoaggregation but Enhance Attachment to Uncoated Surfaces. *Langmuir* **2012**, *28* (9), 4178–4186.
- (37) Rajagopalan, R.; Hiemenz, P. C. Principles of Colloid and Surface Chemistry; CRC Press, 1997.
- (38) Phenrat, T.; Saleh, N.; Sirk, K.; Kim, H.-J.; Tilton, R. D.; Lowry, G. V. Stabilization of aqueous nanoscale zerovalent iron dispersions by anionic polyelectrolytes: adsorbed anionic polyelectrolyte layer properties and their effect on aggregation and sedimentation. *J. Nanopart. Res.* 2008, 10, 795–814.
- (39) He, F.; Zhao, D. Manipulating the size and dispersibility of zerovalent iron nanoparticles by use of carboxymethyl cellulose stabilizers. *Environ. Sci. Technol.* **2007**, *41* (17), 6216–6221.
- (40) Fatisson, J.; Ghoshal, S.; Tufenkji, N. Deposition of carboxymethylcellulose-coated zero-valent iron nanoparticles onto silica: roles of solution chemistry and organic molecules. *Langmuir* **2010**, 26 (15), 12832–12840.
- (41) Mo, Y.; Jin, G.; Zhang, C.; Xu, J.; Tang, H.; Shen, C.; Scheuermann, A.; Li, L. Combined effect of inland groundwater input

- and tides on flow and salinization in the coastal reservoir and adjacent aquifer. *J. Hydrol.* **2021**, *600*, 126575.
- (42) Israelachvili, J. N. Chapter 13 Van der Waals Forces between Particles and Surfaces. In *Intermolecular and Surface Forces*, 3rd ed.; Israelachvili, J. N., Ed.; Academic Press, 2011; pp 253–289.
- (43) Elimelech, M.; O'Melia, C. R. Effect of particle size on collision efficiency in the deposition of Brownian particles with electrostatic energy barriers. *langmuir* **1990**, *6* (6), 1153–1163.
- (44) Tobiason, J. E. Chemical effects on the deposition of non-Brownian particles. *Colloids Surf.* **1989**, 39 (1), 53–75.
- (45) Huang, X.; Bhattacharjee, S.; Hoek, E. M. Is surface roughness a "scapegoat" or a primary factor when defining particle— substrate interactions? *Langmuir* **2010**, *26* (4), 2528–2537.
- (46) Pazmino, E.; Trauscht, J.; Dame, B.; Johnson, W. P. Power law size-distributed heterogeneity explains colloid retention on soda lime glass in the presence of energy barriers. *Langmuir* **2014**, *30* (19), 5412–5421.
- (47) Yao, K.-M.; Habibian, M. T.; O'Melia, C. R. Water and waste water filtration. Concepts and applications. *Environ. Sci. Technol.* **1971**, *5* (11), 1105–1112.
- (48) Torkzaban, S.; Kim, Y.; Mulvihill, M.; Wan, J.; Tokunaga, T. K. Transport and deposition of functionalized CdTe nanoparticles in saturated porous media. *J. Contam. Hydrol.* **2010**, *118* (3–4), 208–217
- (49) Johnson, P. R.; Elimelech, M. Dynamics of colloid deposition in porous media: Blocking based on random sequential adsorption. *langmuir* 1995, 11 (3), 801–812.
- (50) Rajagopalan, R.; Chu, R. Q. Dynamics of adsorption of colloidal particles in packed beds. *J. Colloid Interface Sci.* **1982**, 86 (2), 299–317
- (51) VanNess, K.; Rasmuson, A.; Ron, C. A.; Johnson, W. P. A unified force and torque balance for colloid transport: Predicting attachment and mobilization under favorable and unfavorable conditions. *Langmuir* **2019**, 35 (27), 9061–9070.
- (52) Pazmino, E.; Trauscht, J.; Johnson, W. P. Release of colloids from primary minimum contact under unfavorable conditions by perturbations in ionic strength and flow rate. *Environ. Sci. Technol.* **2014**, 48 (16), 9227–9235.
- (53) Lin, S.; Wiesner, M. R. Deposition of Aggregated Nanoparticles A Theoretical and Experimental Study on the Effect of Aggregation State on the Affinity between Nanoparticles and a Collector Surface. *Environ. Sci. Technol.* **2012**, *46* (24), 13270–13277.
- (54) Zhdanov, S. P.; Kosheleva, L. S.; Titova, T. I. IR Study of Hydroxylated Silica. *Langmuir* **1987**, 3 (6), 960–967.
- (55) Li, Y. S.; Wang, Y. G.; Pennell, K. D.; Abriola, L. M. Investigation of the transport and deposition of fullerene ( $C_{60}$ ) nanoparticles in quartz sands under varying flow conditions. *Environ. Sci. Technol.* **2008**, 42 (19), 7174–7180.
- (56) Hahn, M. W.; O'Melia, C. R. Deposition and reentrainment of Brownian particles in porous media under unfavorable chemical conditions: Some concepts and applications. *Environ. Sci. Technol.* **2004**, 38 (1), 210–220.
- (57) Johnson, W. P.; Tong, M. Observed and simulated fluid drag effects on colloid deposition in the presence of an energy barrier in an impinging jet system. *Environ. Sci. Technol.* **2006**, 40 (16), 5015–5021.
- (58) Griffin, B.; Jurinak, J. Estimation of activity coefficients from the electrical conductivity of natural aquatic systems and soil extracts. *Soil Sci.* **1973**, *116* (1), 26–30.
- (59) Simón, M.; García, I. Physico-chemical properties of the soil-saturation extracts: estimation from electrical conductivity. *Geoderma* **1999**, *90* (1–2), 99–109.
- (60) Adrian, Y. F.; Schneidewind, U.; Bradford, S. A.; Šimůnek, J.; Klumpp, E.; Azzam, R. Transport and retention of engineered silver nanoparticles in carbonate-rich sediments in the presence and absence of soil organic matter. *Environ. Pollut.* **2019**, *255*, 113124.
- (61) Johnson, P. R.; Sun, N.; Elimelech, M. Colloid Transport in Geochemically Heterogeneous Porous Media: Modeling and Measurements. *Environ. Sci. Technol.* **1996**, 30 (11), 3284–3293.

- (62) Kim, H.-J.; Phenrat, T.; Tilton, R. D.; Lowry, G. V. Effect of kaolinite, silica fines and pH on transport of polymer-modified zero valent iron nano-particles in heterogeneous porous media. *J. Colloid Interface Sci.* **2012**, *370* (1), 1–10.
- (63) Sirk, K. M.; Saleh, N. B.; Phenrat, T.; Kim, H.-J.; Dufour, B.; Ok, J.; Golas, P. L.; Matyjaszewski, K.; Lowry, G. V.; Tilton, R. D. Effect of adsorbed polyelectrolytes on nanoscale zero valent iron particle attachment to soil surface models. *Environ. Sci. Technol.* **2009**, 43 (10), 3803–3808.

## ■ NOTE ADDED AFTER ASAP PUBLICATION

Due to a production error, this paper was published ASAP on May 1, 2024, with an error in the TOC/abstract graphic. The corrected version was reposted on May 14, 2024.